Optics Communications 389 (2017) 224–229

Contents lists available at ScienceDirect

Optics Communications

journal homepage: www.elsevier.com/locate/optcom

Lens design for indoor MIMO visible light communications☆

Shang-Bin Li[a,*], Chen Gong[a], Peilin Wang[a], Zhengyuan Xu[a,b]

[a] Laboratory of Wireless-Optical Communications, Chinese Academy of Sciences, University of Science and Technology of China, Hefei, China
[b] Shenzhen Graduate School, Tsinghua University, Shenzhen, China

ARTICLE INFO

Keywords:
Visible light communication
MIMO
Lens design

ABSTRACT

We proposed a lens design procedure to generate parallel light beams that facilitate optical MIMO communication with negligible interference between the un-intended transceiver pairs, in a 2×2 LED array. We designed an imaging receiver using two aspheric lenses instead of one single hemispherical lens to improve the light-beam separation performance. The proposed scheme can be extended to the scenario with ultra-dense LED array. Numerical results show that proper parameter setting in lens design can lead to negligible interference between un-intended transceiver pairs. The bit error rate performance is also evaluated.

1. Introduction

White light emitting diodes (LEDs) serve as good candidates for the indoor visible light communication (VLC) while simultaneously satisfying illumination and communication requirements [1,2]. The most widely used optical modulation and demodulation technology is intensity modulation (IM) and direct detection (DD), where the information bits are carried upon the intensity of the emitted light and received by the photodiodes (PDs) [3]. To further increase the data transmission rates, optical multiple-input multiple-output (MIMO) configurations are adopted to achieve spatial multiplexing (SM) [4–6]. For optical MIMO communication, multiple LEDs transmit modulated signals, which are received by multiple PD modules. Some recent results have been reported in [4–13]. For very high speed VLC, parallel light beams generated via lens between intended transceiver pairs are preferable. To guarantee the low cross-talk between the intended transceiver pairs, delicate optical lens design is required to separate the signals emitted from the transmitting LEDs.

The spatial multiplexing using hemispherical lens has been considered in [11–13]. Note that in [11,12], the spatial multiplexing performance using a flat-surface hemispherical lens is analyzed, for symmetric, asymmetric and tilted arrangement. All existing works can be summarized in the following aspects: (1) all luminaires have one or more LEDs which are regarded as a point source; (2) the hemispherical lens produces distorted images; (3) the transmittance of the hemispherical lens is 100%. Besides, the influence of interference between distinct LED-PD pairs on the communication performance has not been evaluated.

In this work, we propose a lens design procedure to generate parallel light beams that facilitate optical MIMO communication with negligible interference between the un-intended transceiver pairs. More specifically, we consider a 2×2 LED array with very small spacing and a 2×2 PD array with a finite receiving area for each PD. We designed an imaging receiver using two aspheric lenses instead of one single hemispherical lens to improve the light-beam separation performance. The proposed scheme can be extended to the scenario with ultra-dense LED array. We evaluate the light-beam separation for different lens and receiver PD locations. Numerical results show that proper parameter setting in lens design can lead to negligible interference between un-intended transceiver pairs. The bit error rate (BER) performance is also evaluated.

2. Transmission system

2.1. Transmission system configuration

The transmission system is shown in Fig. 1(a), where a LED ceiling light illuminates the room and simultaneously transmits information. The light has a 2×2 LED array, where different LEDs could transmit distinct signals. The receiver consists of two parts, a lens group with two paraboloid lenses for concentrating the emitted light while separating signals from different LEDs, and an array of 2×2 PDs for detecting the optical signals. Let $\boldsymbol{H} \triangleq [H_{ij}]_{1\le i,j\le 4}$ denote the 4×4 channel matrix between the four LEDs and the four PDs, where H_{ij} denotes the

☆ This work was supported by National Key Basic Research Program of China (Grant No. 2013CB329201), Key Program of National Natural Science Foundation of China (Grant No. 61631018), National Natural Science Foundation of China (Grant Nos. 61501420, 61401420), Key Research Program of Frontier Sciences of CAS (Grant No. QYZDY-SSW-JSC003), Key Project in Science and Technology of Guangdong Province (Grant No. 2014B010119001), and Shenzhen Peacock Plan (No. 1108170036003286).

* Corresponding author.
E-mail addresses: shbli@ustc.edu.cn (S.-B. Li), cgong821@ustc.edu.cn (C. Gong), xuzy@ustc.edu.cn (Z. Xu).

http://dx.doi.org/10.1016/j.optcom.2016.12.039
Received 19 July 2016; Received in revised form 16 December 2016; Accepted 18 December 2016
Available online 27 December 2016
0030-4018/

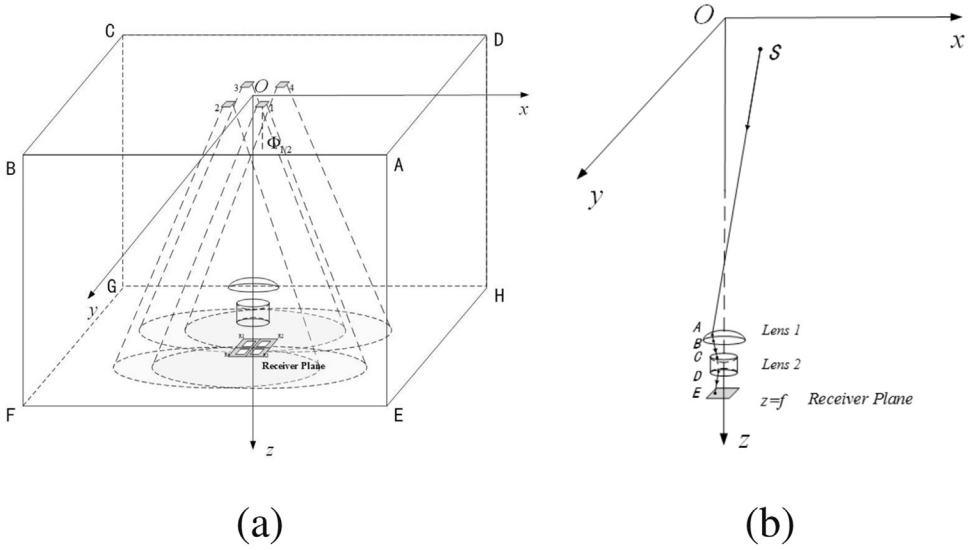

Fig. 1. (a) Schematic diagram of the imaging system configuration; (b) geometrical illustration of the imaging receiver system formed by two aspheric lenses and a PD array.

channel gain between the *i*th PD and the *j*th LED.

Fig. 1(b) demonstrates a geometrical schematic diagram of such a transmission system, illustrating the path of the light refracted by the aspheric lens. Assume that four LEDs form a square array with 40 mm edge length on the *xOy* plane. The LEDs are surface emitting LEDs with the size of 10 mm×10 mm, which emit unpolarized white light directed along positive *Z*-axis. The center of the LED array lies in the origin of the *xOy* plane. The aspheric lens group contains two different lenses. A meniscus lens converges the incident light. It is followed by a biconcave lens that diverges the light. Those refracted rays then hit the PD array in a nearly parallel way. Both two aspheric lenses use parabolic surface for each side. The PD array is located on the imaging plane $Z = 2050$ mm while the two lenses are located at Z=2 m and $Z = 2030$ mm, respectively. The lens positions are firstly roughly inferred from the preset requirement of imaging magnification 1/2 and the imaging law of the compound lenses [15], and then determined via iterative calibration.

2.2. Lens design

In [11,12], a single hemispherical lens has been applied in analyzing the performance of an optical receiver in a MIMO VLC system. However, these schemes may cause the inter-channel crosstalk for an ultra-dense LED array. In this work, we use aspheric lens instead of hemispherical lens to improve the separation of received signals from distinct LEDs. It will be shown that by combining two aspheric lenses, better ray convergence performance could be achieved.

In order to achieve that, we assume that both surfaces of two lenses are parabolic. The even aspheric lens surface can be defined by:

$$z = \frac{cr^2}{1 + \sqrt{1 - (1 + k)c^2r^2}} + \alpha r^2 + \beta r^4 + \cdots, \tag{1}$$

where z is the sag of the even aspheric lens surface, and $r = \sqrt{x^2 + y^2}$ is the radial coordinate of the z-axis rotational symmetric lens surface. Set the radius of curvature c and conic constant k for each lens to be zero to form parabolic shapes. For simplicity in design, only keep the first two terms in the above equation and neglect higher order terms. Thus, the lens parameters to be specified are the front face coefficient $\alpha_i^{(1)}$ and the back face coefficient $\alpha_i^{(2)}$ (i=1,2) for the ith lens. Here we fix the positions of the first and second lens front surface at $Z = 2$ m and $Z = 2030$ mm respectively, and that of the receiver plane at $Z = 2050$ mm. The lens positions are firstly roughly inferred from the preset requirement of imaging magnification 1/2 and the imaging law of the compound lenses [15], and then determined via the iterative calibration. The focal lengths of the first and second lenses should be within the range {25 mm, 35 mm} and {−16 mm, −14 mm} respectively for a good imaging effect. The suitable ranges of the lens parameters can be inferred from the focal lengths. Via Ergodic search we find $\alpha_1^{(1)} \in \{0.035, 0.065\}$, $\alpha_1^{(2)} \in \{0.007, 0.011\}$, $\alpha_2^{(1)} \in \{-0.08, 0\}$, $\alpha_2^{(2)} \in \{0.01, 0.1\}$. In order to determine the parameters of the lenses, we adopt the Zemax software to repeatedly numerically simulate the channel matrices between the LED array and the PD array via automatically varying the parameters of the lenses within the pre-determined ranges, and then obtain their corresponding singular value decompositions (SVDs). The more uniform singular values of the MIMO channel matrix imply the larger MIMO gain of the lenses designed. Thus the iterative optimization procedure of the lens design is to maximize the SVD's uniformity. The first lens is designed as meniscus shape with $\alpha_1^{(1)} = 0.038$ and $\alpha_1^{(2)} = 0.01$ in order to converge incident light; and the second lens is designed as biconcave shape with $\alpha_2^{(1)} = -0.060$ and further $\alpha_2^{(2)} = 0.06$ so as to separate light from distinct LED sources. As shown in the Appendix, the slight disturbance of the optimized lens parameters would significantly degrade the signal separation performance. Besides, it should be noted that the reference coordinate of the aspheric surfaces formula is the center of the front face. The indices of refraction for both lenses are set to be 1.50, a typical number of common glass materials. Table 1 shows the optimized parameters of this lens group obtained in the simulations, in which the radius aperture and the thickness of the lenses are sophisticatedly given. The optimization of the position of the second lens and the face coefficients of both lenses are conducted jointly while the position of the first lens is fixed at $Z = 2$ m. In the numerical part, we show the ray separation performance for different lens locations.

3. Numerical results

We simulate a single imaging receiver system with a 2×2 white light LED transmitter array installed on the ceiling pointing down as shown

Table 1
Parameters of the components of the imaging receiver.

	$\alpha_1^{(1)}$, $\alpha_2^{(1)}$	$\alpha_1^{(2)}$, $\alpha_2^{(2)}$	Radius aperture (mm)	Thickness (mm)
Lens 1	0.038	0.01	15	6.3
Lens 2	−0.060	0.06	10	2

Table 2
Channel gains with varying half power semi-angles.

$\Phi_{1/2}$	5°	15°	45°	60°
Gain	7.00×10^{-4}	8.21×10^{-5}	1.19×10^{-5}	7.46×10^{-6}

in Fig. 1(a). Assume that the room height is 3 m. Four LEDs are installed symmetrically at $T_x^{(1)}$: (20, 20, 0), $T_x^{(2)}$: (20, −20, 0), $T_x^{(3)}$: (−20, −20, 0) and $T_x^{(4)}$: (−20, 20, 0) in millimeters. The center of the PD array is positioned at R: (0, 0, 2050). It can be demonstrated that the curved-surface receiver as shown in Fig. 1(b) provides larger channel gains than the flat-surfaced. Thus, we put the front surface of the first lens as curved-surface to get a larger channel gain. All the simulations are based on the non-sequential mode of the optical analysis software Zemax.

3.1. Channel gain of SISO imaging system

The channel gain in MIMO VLC [3], denoted as T, is determined by the ratio of the received power P_0 at the PD and the transmitted power P_t of the LED, i.e.

$$T = P_0/P_t. \quad (2)$$

For simplicity the channel gain of a single-input single-output (SISO) VLC system is investigated here where only one LED-PD pair is operating as shown in Fig. 1(b), for different photometries of the transmitters. The receiving area of the single PD is 1 mm×1 mm. In Table 2, the SISO imaging system channel gains on the receiver plane are shown for four typical values of $\Phi_{1/2}$, 5°, 15°, 45° and 60° of Lambertian LEDs, where the first and second lenses are fixed at Z=2 m and Z = 2030 mm respectively. The channel gain decreases significantly with the increase of the value of $\Phi_{1/2}$. The results of channel gain under different $\Phi_{1/2}$ provide us a reference about the amplification performance and the path loss due to the designed optical system.

3.2. Power distribution with stationary lens positions

Now we turn to the MIMO system with a 2×2 LED array located at $T_x^{(1)}$, $T_x^{(2)}$, $T_x^{(3)}$, and $T_x^{(4)}$. The center of the receiver is located at R: (0, 0, 2050), and each PD is aligned symmetrically around R but the distance between each pair of detectors still needs to be determined via simulations.

The power distribution on the detector plane for different lens locations can be investigated. Assuming the front surface of the first lens (meniscus lens) is fixed at Z=2 m, we evaluate the power distribution with respect to different locations of the second lens. For

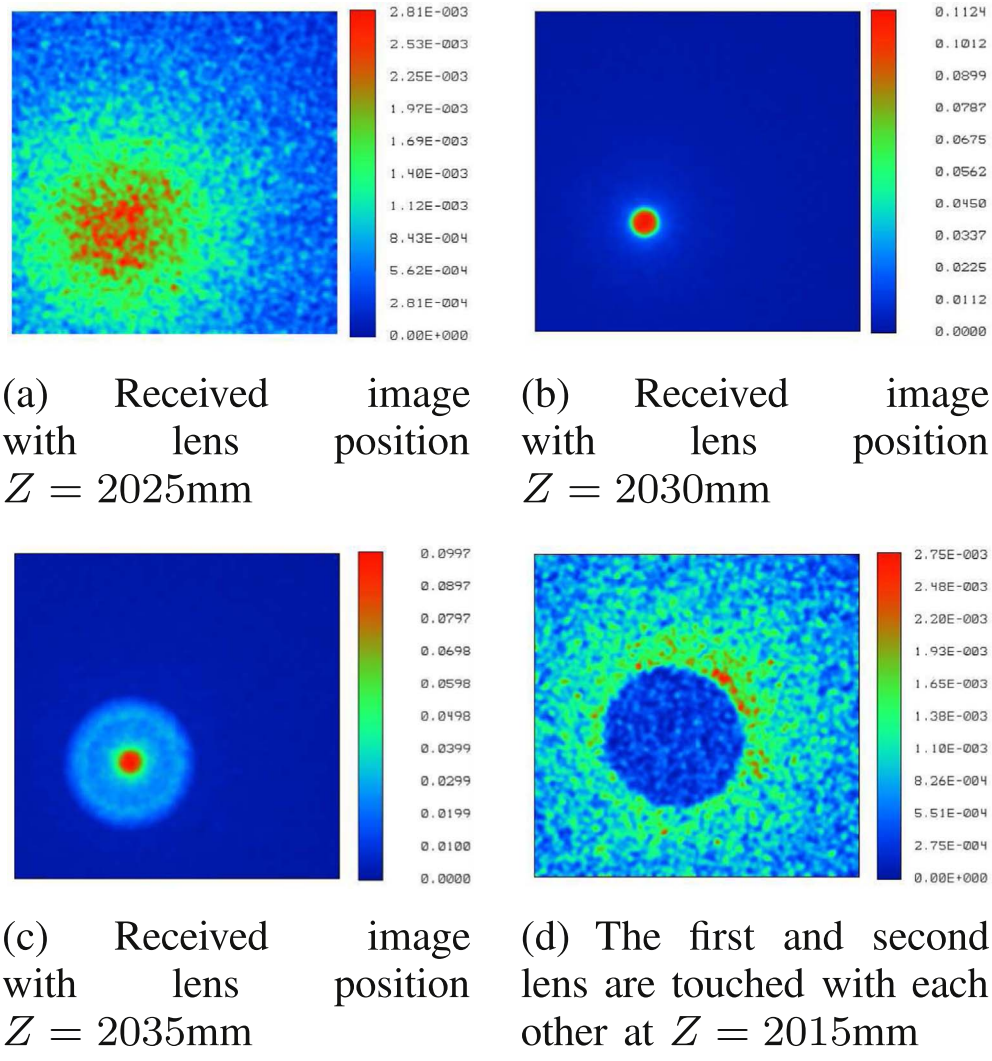

(a) Received image with lens position $Z = 2025$mm

(b) Received image with lens position $Z = 2030$mm

(c) Received image with lens position $Z = 2035$mm

(d) The first and second lens are touched with each other at $Z = 2015$mm

Fig. 2. Received image with different lens positions. The size of the receiving plane is 8 mm×8 mm with its center located at R: (0, 0, 2050).

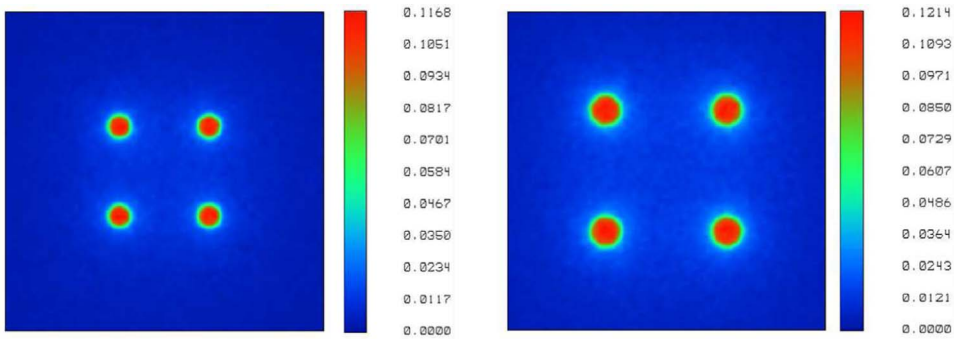

(a) Received image for $Z = 1750\text{mm}$; (b) Received image for $Z = 2350\text{mm}$;

Fig. 3. Received image with different receiver systems' positions (a) detector plane at $Z = 1750$ mm; (b) detector plane at $Z = 2350$ mm. The size of the receiving plane is 8 mm×8 mm.

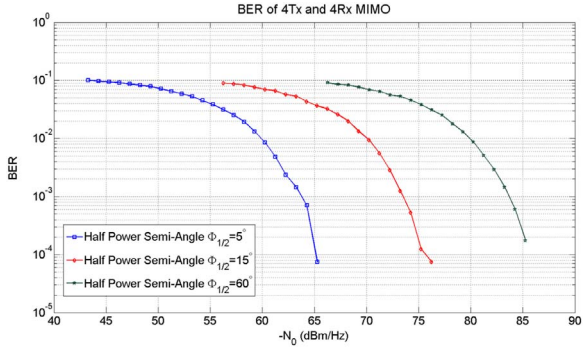

Fig. 4. BER performance of designed imaging receiver with different LED half power semi-angles but the same values 1 W of transmitted optical power.

simplicity we only consider the case where $\Phi_{1/2} = 5°$. Fig. 2 plots the power distribution with the position of the second lens at $Z = 2025$ mm, $Z = 2030$ mm and $Z = 2035$ mm, respectively. It is seen that the best imaging result is achieved when the lens is located at $Z = 2030$ mm. Either shorter ($Z = 2025$ mm case) or longer ($Z = 2035$ mm case) distance from the image plane would incur nonuniform power distribution and hence poor separation of signals from different LEDs. Besides the above positions we also checked a range of values from $Z = 2015$ mm to $Z = 2040$ mm and find that only when $Z = 2030$ mm the received power distribution can be uniform and separable.

3.3. Power distribution with symmetrical arrangement

Firstly consider the narrow beam case where $\Phi_{1/2} = 5°$. Obviously, the images of the four LEDs $T_x^{(1)}$, $T_x^{(2)}$, $T_x^{(3)}$, and $T_x^{(4)}$ will mainly be projected on the third, the second, the first and the fourth PD, respectively, if the centers of the four 1 mm×1 mm PDs are placed at the square corners with edge length of 3 mm. We need to look at the channel matrix we obtained to see whether the signals transmitted from each light source can be easily distinguished. The normalized channel matrix can be calculated via calculating received optical power over each PD, given as follows:

$$\boldsymbol{H} = \begin{pmatrix} 0.0192 & 0.0322 & 1.0122 & 0.0335 \\ 0.0354 & 0.0185 & 0.0335 & 0.9976 \\ 1.0008 & 0.0338 & 0.0203 & 0.0320 \\ 0.0359 & 0.9894 & 0.0374 & 0.0240 \end{pmatrix} \times 10^{-4}, \tag{3}$$

where the (i, j)th element H_{ij} represents the received optical power of the image of the jth LED over the ith PD. Clearly, the matrix has a dominant element in each row, meaning that there is one strongest link among four links connecting four LEDs to their corresponding detectors which can be viewed as main channel. It thus causes negligible crosstalk or interference between different LEDs in the receiver plane, resulting in well separation of the four LED images. From the communication viewpoint, the four sub-channels have little interference with each other since the most part of the transmitted optical power from one light source is concentrated in only one specific channel link connecting the source and its corresponding receiver. The channel condition can be revealed through the singular values of this channel matrix. The corresponding SVD of the channel matrix gives its four singular values as $\{1.0893, 0.9871, 0.9728, 0.9508\} \times 10^{-4}$. They are close to each other. To show the uniformity of channel matrix, it may be more clear to show the condition number defined as the ratio between the largest and smallest singular values. For the channel matrix in Eq. (3), the condition number is 1.1457.

The optical power distribution performances of medium beam ($\Phi_{1/2} = 15°$) and wide beam ($\Phi_{1/2} = 45°$, $60°$) LEDs are also simulated and analyzed, and the concentrations of the four LED images remain separable, with negligible interference between different LEDs. The channel matrices for $\Phi_{1/2} = 15°$ and $60°$ are given as follows:

$$\boldsymbol{H} = \begin{pmatrix} 0.0150 & 0.0382 & 0.9683 & 0.0259 \\ 0.0177 & 0.0164 & 0.0341 & 1.0147 \\ 0.9928 & 0.0286 & 0.0205 & 0.0368 \\ 0.0341 & 1.0242 & 0.0273 & 0.0218 \end{pmatrix} \times 10^{-5}, \quad \text{for } \Phi_{1/2} = 15°; \tag{4}$$

Table 3
Key parameters comparison between the aspheric lens imaging system and the hemispherical lens imaging system used in [13].

Lens type	LED size	LED interval	PD size	PD interval	BER (SNR=10 dB)	BER (SNR=15 dB)
Aspheric	10 mm	40 mm	1 mm	1.5 mm	3.1×10^{-2}	4.8×10^{-3}
Hemispherical (curved)	Point source	3 m	5 mm	0 mm	4×10^{-1}	4×10^{-1}
Hemispherical (flat)	Point source	3 m	5 mm	0 mm	1×10^{-1}	5×10^{-2}

$$\boldsymbol{H} = \begin{pmatrix} 0.0184 & 0.0368 & 0.9996 & 0.0322 \\ 0.0343 & 0.0205 & 0.0336 & 1.0230 \\ 0.9879 & 0.0336 & 0.0256 & 0.0263 \\ 0.0358 & 0.9894 & 0.0358 & 0.0139 \end{pmatrix} \times 10^{-6}, \quad \text{for } \Phi_{1/2} = 60^\circ, \tag{5}$$

and their corresponding singular values and condition numbers are $\{1.0830, 1.0000, 0.9704, 0.9467\} \times 10^{-5}$, 1.1440, and $\{1.088, 0.9932, 0.9718, 0.9470\} \times 10^{-6}$, 1.1489 respectively.

3.4. Power distribution of mobile imaging system

We also studied the optical power distribution for different Z-axis positions of the optical receiver system, under the assumption of fixed relative positions of all components inside the optical receiver as specified in Section 3.2 to see whether this optical receiver system is robust to moderate movement in vertical direction. For the case where half power semi-angle $\Phi_{1/2} = 60^\circ$, Fig. 3 shows the received images when the detectors plane is located at $Z = 1750$ mm and $Z = 2350$ mm, respectively. It is shown that when the receiver is moved upwards or downwards along the Z-axis, the images can still be well separated. After several simulations we define the movable range of this system in vertical direction to be from $Z = 1500$ mm to $Z = 2500$ mm. In other words, the separation of the four LEDs is not sensitive to the Z-directional location of the optical receiver. However, this optical MIMO receiver system is sensitive to the horizontal movement. In those application scenarios of the VLC which need the horizontal mobility, uniform luminance is preferred, and the field of view of the receiver is also critical factor for mobility [16].

3.5. BER performance of the imaging system

According to the channel matrix obtained in Section 3.3, and assuming on–off keying (OOK) modulation for the LED array and the maximum likelihood detection at the PD array [13,14], the BER performance with respect to different LED half power semi-angles is plotted in Fig. 4, where N_0 is the average two-sided power spectral density of the additive white Gaussian noise of the 4 channels. Due to the negligible crosstalk between the LEDs, the BER significantly decreases for large SNR. Also note that, for the same BER and noise level, larger transmitted optical power is required for larger half power semi-angle. Table 3 shows the BER comparisons between the aspheric lens and the hemispherical lens. Note that the advantage of the present optical design of the receiver is its high resolution (angle of minimum resolution is smaller than 0.6°) for the 4×4 MIMO VLC which implies the designed receiver can be scalable and applied to the 16×16 MIMO VLC with the size constraint 100 mm×100 mm of both the transmitters and the receivers. However, it is very difficult to simultaneously satisfy the high resolution and the large field of view of the receiver. For the 3 m separated LED array, the hemispherical lens may be the better choice.

4. Conclusions

In this paper, we have shown the feasibility of using a set of aspheric lenses to separate the 2×2 LED array beam for indoor MIMO VLC applications. A set of aspheric lenses are designed and the relative position between lenses is analyzed for better spatial diversity. Numerical results on various different LED photometries, including the channel gain, inter-channel crosstalk, and the corresponding BER have been provided. The lens design for ultra-dense MIMO VLC with more transceiver pairs remains for future research.

Appendix

The SVD of the 4×4 MIMO channel matrix can explicitly reveal its inter-channel crosstalk, and the more uniform singular values imply the better parallel channel conditions and larger MIMO gain. In the following, it is shown that slight disturbance of the optimized lens parameters shown in Section 2 would significantly degrade the signal separation performance. The corresponding singular values, the condition number and the channel matrices for $\Phi_{1/2} = 5^\circ$ for the following four parameter settings are

(1) $\alpha_1^{(1)} = 0.05$, $\alpha_1^{(2)} = 0.01$, $\alpha_2^{(1)} = -0.06$, $\alpha_2^{(2)} = 0.06$: $\{1.4283, 0.8888, 0.8728, 0.8102\} \times 10^{-4}$, 1.6817;

$$\boldsymbol{H} = \begin{pmatrix} 0.0764 & 0.1512 & 0.9966 & 0.1350 \\ 0.1360 & 0.0833 & 0.1330 & 0.9931 \\ 0.9946 & 0.1261 & 0.0764 & 0.1281 \\ 0.1429 & 1.0158 & 0.1394 & 0.0635 \end{pmatrix} \times 10^{-3};$$

(2) $\alpha_1^{(1)} = 0.038$, $\alpha_1^{(2)} = 0.0$, $\alpha_2^{(1)} = -0.06$, $\alpha_2^{(2)} = 0.06$: $\{1.5913, 0.8307, 0.7943, 0.7838\} \times 10^{-4}$, 1.6880;

$$\boldsymbol{H} = \begin{pmatrix} 0.0820 & 0.1346 & 1.0103 & 0.1469 \\ 0.1347 & 0.0813 & 0.1429 & 0.9860 \\ 1.0021 & 0.1318 & 0.0815 & 0.1349 \\ 0.1369 & 1.0016 & 0.1420 & 0.0794 \end{pmatrix} \times 10^{-3};$$

(3) $\alpha_1^{(1)} = 0.038$, $\alpha_1^{(2)} = 0.01$, $\alpha_2^{(1)} = -0.1$, $\alpha_2^{(2)} = 0.06$: $\{1.2273, 0.9574, 0.9379, 0.8773\} \times 10^{-4}$, 2.1524;

$$\boldsymbol{H} = \begin{pmatrix} 0.1324 & 0.1967 & 0.9798 & 0.2020 \\ 0.2015 & 0.1416 & 0.2078 & 0.9914 \\ 1.0110 & 0.2155 & 0.1392 & 0.2001 \\ 0.2255 & 1.0182 & 0.2121 & 0.1363 \end{pmatrix} \times 10^{-3};$$

(4) $\alpha_1^{(1)} = 0.038$, $\alpha_1^{(2)} = 0.01$, $\alpha_2^{(1)} = -0.06$, $\alpha_2^{(2)} = 0.0$: $\{1.1284, 0.9731, 0.9638, 0.9347\} \times 10^{-4}$, 2.8264.

$$\boldsymbol{H} = \begin{pmatrix} 0.1688 & 0.2939 & 1.0223 & 0.2740 \\ 0.2801 & 0.2141 & 0.2748 & 0.9762 \\ 1.0177 & 0.2801 & 0.2057 & 0.3162 \\ 0.2740 & 0.9839 & 0.2916 & 0.1995 \end{pmatrix} \times 10^{-3};$$

References

[1] J.R. Barry, J.M. Kahn, E.A. Lee, D.G. Messerschmitt, High-speed nondirective optical communication for wireless networks, IEEE Netw. Mag. 5 (November (6)) (1991) 44–54.

[2] T. Komine, M. Nakagawa, Fundamental analysis for visible-light communication system using LED lights, IEEE Trans. Consum. Electron. 50 (February) (2004) 100–107.

[3] J.M. Kahn, J.R. Barry, Wireless infrared communications, Proc. IEEE 85 (February (2)) (1997) 265–298.

[4] L. Zeng, D.C. O'Brien, H.L. Minh, G.E. Faulkner, K. Lee, D. Jung, Y. Oh, E.T. Won, High data rate multiple input multiple output (MIMO) optical wireless communications using white LED lighting, IEEE J. Sel. Areas Commun. 27 (December (9)) (2009) 1654–1662.

[5] A.H. Azhar, T.-A. Tran, D.C. O'Brien, A gigabit/s indoor wireless transmission using MIMO-OFDM visible-light communications, IEEE Photon. Technol. Lett. 25 (January (2)) (2013) 171–174.

[6] K.D. Dambul, D.C. O'Brien, G. Faulkner, Indoor optical wireless MIMO system with an imaging receiver, IEEE Photon. Technol. Lett. 23 (January (2)) (2011) 97–99.

[7] X. Zhang, K. Cui, H. Zhang, Z. Xu, Capacity of MIMO visible light communication channels, in: IEEE Photonics Society Summer Topical Meeting, July 2012, pp. 159–160.

[8] S. Hranilovic, F.R. Kschischang, A pixelated MIMO wireless optical communication system, IEEE J. Sel. Top. Quantum Electron. 12 (August (4)) (2006) 859–874.

[9] S.D. Perli, N. Ahmed, D. Katabi, PixNet: interference-free wireless links using LCD-Camera pairs, in: Proceedings of the MOBICOM2010, Chicago, 2010 pp. 137–148.

[10] A. Burton, H. Le Minh, Z. Ghassemlooy, E. Bentley, C. Botella, Experimental demonstration of 50-Mb/s visible light communications using 4×4 MIMO, IEEE Photon. Technol. Lett. 26 (May (9)) (2014) 945–948.

[11] T.Q. Wang, Y.A. Sekercioglu, J. Armstrong, Hemispherical lens based imaging receiver for MIMO optical wireless communications, in: Proceedings of the 3rd IEEE Workshop on Optical Wireless Communications, Anaheim, CA, December 2012, pp. 1239–1243.

[12] T.Q. Wang, Y.A. Sekercioglu, J. Armstrong, Analysis of an optical wireless receiver using a hemispherical lens with application in MIMO visible light communications, J. Lightwave Technol. 31 (June (11)) (2013) 1744–1754.

[13] B. Li, X. Lai, J. Wang, X. Liang, C. Zhao, Performance analysis of the imaging receivers using a hemispherical lens for visible light communications, in: 2013 International Conference on Wireless Communications and Signal Processing, October 2013, pp. 1–5.

[14] H.L. Minh, D.C. O'Brien, G. Faulkner, L. Zeng, K. Lee, D. Jung, Y. Oh, High-speed visible light communications using multiple-resonant equalization, IEEE Photon. Technol. Lett. 20 (July (15)) (2008) 1243–1245.

[15] E. Hecht, Optics, 4th ed., San Francisco, Addison Wesley, 2002

[16] A. Burton, H. Le Minh, Z. Ghassemlooy, S. Rajbhandari, A study of LED lumination uniformity with mobility for visible light communications, in: IWOW 2012: International Workshop on Optical Wireless Communications, Pisa, Italy, October 2012, pp. 1–3.